

Freeze-in Dark Matter Through Forbidden Channel in $U(1)_{B-L}$

Partha Konar,^a Rishav Roshan,^a Sudipta Show^{a,b}

^aPhysical Research Laboratory, Ahmedabad - 380009, Gujarat, India

^bIndian Institute of Technology, Gandhinagar - 382424, Gujarat, India

E-mail: konar@prl.res.in, rishav@prl.res.in, sudipta@prl.res.in

Abstract. We examine a scenario for freeze-in production of dark matter, which occurs due to the large thermal correction to the mass of a decaying mediator particle present in the thermal bath of the early Universe. We show that the decays, which are kinematically forbidden otherwise, can open up at very high temperatures and dominate the dark matter production. We explore such forbidden production of dark matter in the minimal $U(1)_{B-L}$ model, comparing dark matter phenomenology in the context of forbidden frozen-in with the standard picture.

Keywords: Freeze-in, Dark matter, Thermal correction

Contents

1	Introduction	1
2	The scenario	3
3	Thermal corrections	6
4	Theoretical and experimental constraints	7
4.1	Theoretical constraints	7
4.2	Experimental Constraints	7
5	Dark Matter Phenomenology	8
5.1	Case A: Complete FFI region when $M_{Z_{BL}} > M_1 > m_s$	11
5.2	Case B: Partial FFI region when $M_{Z_{BL}} > m_s > M_1$	13
6	Summary and conclusions	15

1 Introduction

The existence of a non-luminous and non-baryonic form of matter popularly known as dark matter (DM) is already well established by the observations like galaxy rotation curve [1], Bullet cluster [2], etc. Besides, the amount of dark matter at present has been measured quite precisely in the experiments like Planck [3], WMAP [4] by using the Standard Model of cosmology, i.e., the Λ CDM model. However, the exact nature of dark matter and its production mechanism remain a mystery and an open question. Since the Standard Model(SM) fails to provide a viable DM candidate, one needs to go beyond the Standard Model(BSM) of particle physics in order to accommodate a feasible dark matter.

Among the existing dark matter models, the most popular ones are those that accommodate dark matter in the form of the weakly interacting massive particle (WIMP) [5–14]. Here, the DM interactions with the SM lies in the weak scale. In the early Universe, such a kind of DM remained in thermal equilibrium with the hot and dense SM plasma. When the temperature of the Universe cooled and fell below its mass, its number density started to dilute, which continued till the time its annihilation rate became smaller than the expansion rate of the Universe. Subsequently, its number density freezes out, and the resulting yield gets saturated. Interestingly, the dynamics of the freeze-out mechanism can also be affected once the thermal corrections are incorporated, as shown in [15]. An exciting aspect of the freeze-out is that it is dominated by physics at low energies, as it occurs near a temperature that is 20 - 25 times smaller than the DM mass. Hence the formation mechanism does not carry any information about the history of the early Universe.

Despite such interesting features, the WIMP paradigm still remains in tension due to its null detection at various direct [16–18], indirect [19] and collider [20, 21] frontiers. These null results motivate us to explore various other possibilities of DM production. Among them, the most popular one is the freeze-in production of the DM from the thermal bath. Here, one assumes: (i) a negligible initial abundance of DM in the early Universe and (ii) a very feeble interaction of the DM with the thermal plasma. Such feeble interactions are responsible for

the gradual production of DM from the decay or scattering of the bath particles. Furthermore, the smallness of the same interactions also ensures that the DM never thermalizes with the bath. Once the number density of the particles responsible for the DM production becomes Boltzmann suppressed, the comoving number density of the DM ceases, and its abundance freezes in. This type of DM is popularly known as *feebly interacting massive particle* or FIMP [22, 23]. Depending on the nature of DM interactions with thermal bath, the freeze-in scenario can be categorized as (i) the Ultra-Violet (UV) freeze-in [22, 24–27] and (ii) the Infrared (IR) freeze-in [22, 23, 28–31]. In a UV freeze-in scenario, the DM interacts with the bath particles only via non-renormalizable (*i.e.*, higher dimensional) operators. In this picture, dark matter is produced solely through the scattering of the bath particles in the early Universe, and the dark matter abundance is highly sensitive to physics at high temperatures, particularly to the reheating temperature of the Universe. Contrary to the UV freeze-in, in IR freeze-in, the dark matter is connected with the visible sector only via renormalizable interaction. Here, dark matter production is dominated primarily at the temperature around the mass of the heavier particle involved in the interactions.

In this work, we focus on DM production, where it has renormalizable interactions with the thermal bath (IR freeze-in). From here onwards, we will refer to the freeze-in scenario where the DM production dominantly takes place at a temperature near about the mass of the decaying¹ bath particle as a *standard freeze-in* or SFI. Deviating from this scenario, in the present analysis, we consider the production of DM in a parameter regime where its production remains kinematically forbidden in the SFI framework. Darmé et al. studied such a mechanism recently for DM production in Ref. [32]. The interesting feature of this particular production mechanism is the involvement of thermally corrected masses [32–38] of the particles participating in the DM production. Here, one considers that the mediator is not only a part of the hot thermal plasma, but it may also acquire a sizable thermal mass. In the early Universe, when the temperature was extremely high, the thermal mass of the mediator can have differed substantially from its mass at vacuum, *i.e.*, the thermal effects must have dominated the mediator’s mass. Analogous to the SFI, here, the initial population of dark matter is assumed to be zero or negligibly small, and it is produced gradually from the mediator’s decay. At a sufficiently high temperature, the mediator can acquire large thermal mass, and the condition: $M_{\text{mediator}}(T) > 2M_{\text{DM}}$ can easily be achieved. The dark matter then can be copiously produced from this decay, even if such a process remains kinematically forbidden at low temperatures. This alternative approach of DM production can be indexed as *forbidden freeze-in* (FFI). This new FFI scenario can open up an exciting and new paradigm of dark matter phenomenology.

This article aims to explore the FFI scenario in a minimal $U(1)_{B-L}$ extension [28, 39–47] of the SM. As is well known, the $B - L$ extension necessitates the introduction of three right-handed neutrinos (RHN) to make the model free from the triangular anomaly. Unlike the Type-I seesaw [48–54], here, the bare mass term for the RHNs are not allowed at tree level. Hence, in order to make the RHNs massive, they are required to couple to an SM gauge singlet (complex) scalar appropriately charged under the $U(1)_{B-L}$ symmetry. These RHNs become massive once the $B - L$ scalar acquires a non-zero vacuum expectation value (vev) and spontaneously breaks the $U(1)_{B-L}$ symmetry. In addition, the $B - L$ gauge boson also becomes massive after the breaking of $B - L$ symmetry. It is interesting to point out that the $B - L$ setup can provide a common solution to three of the most important issues of present-

¹Assuming the production of the DM through the scattering of the bath particles remains sub-dominant in comparison the production via decay.

Field	$SU(2)_L \times U(1)_Y$	Y_{BL}	\mathbb{Z}_2
N_1	(1, 0)	-1	-
N_2, N_3	(1, 0)	-1	+
S	(1, 0)	2	+

Table 1: The additional fields and their quantum numbers under different symmetry groups. Here, Y_{BL} refers to the $U(1)_{B-L}$ charge.

day particle physics and cosmology, *i.e.*, the non-zero neutrino mass [9, 54–58], baryogenesis via leptogenesis [9, 59–64] from the decay of heavier RHNs and dark matter (WIMP/FIMP). The WIMP type DM in the context of the $B - L$ extension has been thoroughly studied [6, 65, 66]. Here, the lightest RHN (non-trivially charged under a Z_2 symmetry) plays the role of a DM [67]. Even though such extension can explain all three outstanding issues under the same umbrella, the DM phenomenology still remains highly constrained. The RHN dark matter relic density can only satisfy the Planck limit [3] near the resonance regimes [65, 66]. An interesting alternative is to consider the lightest RHN as FIMP type DM (SFI). This possibility is also vastly explored in the literature [6, 28, 43, 44, 68, 69] and unlike the WIMP scenario, here a sizable mass range is allowed² for DM. Contrary to this, in the present setup, we follow the FFI approach to study the freeze-in production of dark matter from the kinematically disallowed decay of the scalar that gets a significant thermal mass correction while maintaining equilibrium with the hot thermal plasma in the early Universe.

This paper is organized as follows. In Section 2, we introduce the model part while Section 3 describes in detail the thermal mass correction of the mediator. Different theoretical and experimental constraints deemed relevant here are described in Section 4. Next, we present the forbidden freeze-in production of dark matter and the estimation of numerical results in Section 5 and finally, we summarize our findings in Section 6.

2 The scenario

The present scenario explores the possibility of a $U(1)_{B-L}$ extension of the SM gauge symmetry. Here, the particle content is extended by adding three right-handed neutrinos N_i ($i = 1, 2, 3$) together with a complex scalar S , all of them charged under the $U(1)_{B-L}$ symmetry. In addition, the SM leptons and quarks also carry $U(1)_{B-L}$ charges of -1 and $+\frac{1}{3}$, respectively. Further, invoking an additional unbroken discrete Z_2 symmetry and making one of the RHN (say, N_1) non-trivially charged under it ensures its stability by forbidding its interactions with the SM leptons and Higgs. Being stable, N_1 contributes as a suitable DM candidate in the present setup. On the other hand, the remaining BSM particles and SM particles carry a positive charge under this Z_2 . In Table 1, we present the charges of all the BSM fields under the different symmetry groups.

These $B - L$ charge assignments also eliminate the possibility of triangular $B - L$ gauge anomalies in our model [71]. With the given particle spectrum and the gauge symmetries, the most general renormalizable and gauge invariant Lagrangian for the present setup can be written as,

²We would like to point out that in a recent study [70], the authors have shown that Lyman- α bound can also exclude DM mass $\lesssim \mathcal{O}(15 \text{ keV})$ if produced through a freeze-in mechanism.

$$\mathcal{L} = \mathcal{L}_{KE} + \mathcal{L}_y - V(\phi, S) \quad (2.1)$$

where kinetic terms \mathcal{L}_{KE} for the BSM fields are given as,

$$\mathcal{L}_{KE} = |D_\mu S|^2 + \sum_{i=1,2,3} \bar{N}_i i \gamma^\mu D_\mu N_i - \frac{1}{4} Z_{\mu\nu} Z^{\mu\nu}, \quad (2.2)$$

with $Z^{\mu\nu} = \partial^\mu Z_{BL}^\nu - \partial^\nu Z_{BL}^\mu$, and $D_\mu = \partial_\mu + i[Yg' + Y_{BL}g_{BL}](Z_{BL})_\mu$. Here, we work in the pure $U(1)_{B-L}$ model, where g' is considered to be zero. This choice of $g' = 0$ forbids Z - Z_{BL} mixing at the tree level³. Finally, g_{BL} denotes the $U(1)_{B-L}$ gauge coupling.

Moving on to the scalar part of the Lagrangian, the most general renormalizable scalar potential for this setup is given by

$$V(\phi, S) = -\mu_\phi^2 \phi^\dagger \phi - \mu_S^2 |S|^2 + \frac{\lambda_\phi}{2} (\phi^\dagger \phi)^2 + \lambda_{\phi S} (\phi^\dagger \phi) |S|^2 + \lambda_S |S|^4. \quad (2.3)$$

For $\mu_S^2 > 0$, the CP even component of $B-L$ scalar $S = \frac{1}{\sqrt{2}}(v_{BL} + \phi_S)$ develops a non-zero vacuum expectation value v_{BL} and breaks the $U(1)_{B-L}$ symmetry. This breaking ensures Majorana masses for the RHNs (discussed latter) together with an additional massive $B-L$ gauge boson Z_{BL} . The masses of the $B-L$ scalar (ϕ_S) and gauge boson after the $B-L$ symmetry breaking is expressed as⁴,

$$m_S^2 = 2\lambda_S v_{BL}^2, \quad (2.4a)$$

$$M_{Z_{BL}} = 2g_{BL} v_{BL}. \quad (2.4b)$$

On the other hand, Electroweak Symmetry Breaking (EWSB) is triggered for μ_ϕ^2 when the CP-even components of ϕ receive a vev v . The minimization conditions for the potential in Eq. 2.3 are given below:

$$\mu_\phi^2 = \frac{\lambda_\phi}{2} v^2 + \frac{\lambda_{\phi S}}{2} v_{BL}^2, \quad (2.5a)$$

$$\mu_S^2 = \frac{\lambda_{\phi S}}{2} v^2 + \lambda_S v_{BL}^2. \quad (2.5b)$$

After the EWSB, scalar doublet in the present setup can be parametrized as

$$\phi = \begin{pmatrix} 0 \\ \frac{1}{\sqrt{2}}(v + \phi_h) \end{pmatrix}. \quad (2.6)$$

Subsequent to the EWSB, a non-zero $\phi_h - \phi_S$ mixing leads to the following mass terms

$$V \supset \frac{1}{2} (\phi_h \ \phi_S) \begin{pmatrix} \lambda_\phi v^2 & \lambda_{\phi S} v v_{BL} \\ \lambda_{\phi S} v v_{BL} & 2\lambda_S v_{BL}^2 \end{pmatrix} \begin{pmatrix} \phi_h \\ \phi_S \end{pmatrix}. \quad (2.7)$$

³The gauge kinetic mixing is highly constrained by electroweak precision measurements demands it to be $\lesssim 10^{-4}$ [72].

⁴After the breaking of $B-L$ symmetry, ϕ also obtains mass due to the presence of $\lambda_{\phi S}$ interaction. We do not write that mass term explicitly as its presence does not alter the present analysis.

The mass matrix is diagonalised using

$$\begin{pmatrix} \phi_h \\ \phi_S \end{pmatrix} = \begin{pmatrix} c_\theta & s_\theta \\ -s_\theta & c_\theta \end{pmatrix} \begin{pmatrix} h \\ s \end{pmatrix} \quad (2.8)$$

with

$$\tan 2\theta = \frac{-2\lambda_{\phi S} v v_{BL}}{\lambda_\phi v^2 - 2\lambda_S v_{BL}^2}. \quad (2.9)$$

The mass eigenstates (h, s) then have masses

$$m_{h,s}^2 = \frac{1}{2} \left[(\lambda_\phi v^2 + 2\lambda_S v_{BL}^2) \pm \sqrt{(\lambda_\phi v^2 - 2\lambda_S v_{BL}^2)^2 + 4\lambda_{\phi S}^2 v^2 v_{BL}^2} \right]. \quad (2.10a)$$

Here we consider physical scalar h as the SM like Higgs boson with mass $m_h = 125.09$ GeV [73]. The various model parameters are expressible in terms of the physical quantities as follows:

$$\lambda_\phi = \frac{(m_h^2 c_\theta^2 + m_s^2 s_\theta^2)}{v^2}, \quad (2.11a)$$

$$\lambda_{\phi S} = \frac{(m_s^2 - m_h^2) s_\theta c_\theta}{v v_{BL}}, \quad (2.11b)$$

$$\lambda_S = \frac{(m_h^2 s_\theta^2 + m_s^2 c_\theta^2)}{2v_{BL}^2}. \quad (2.11c)$$

The $\phi_S - \phi_h$ mixing angle is highly constrained, and the current experiments demand it to be small (see Section 4). As this mixing angle does not play any significant role in the present context, we have kept s_θ fixed at 10^{-3} throughout this work, such that it satisfies the experimental constraints. In the limit of sufficiently small $\phi_S - \phi_h$ mixing, one obtains $\phi_S \simeq s$, and $m_S \simeq m_s$.

Next, the Yukawa interactions for the present scenario is expressed as,

$$-\mathcal{L}_y \supset y_{11} \bar{N}_1^c N_1 S + y_{\alpha\beta} \bar{N}_\alpha^c N_\beta S + h_{i\alpha} \bar{l}_L \tilde{\phi} N_\alpha + h.c., \quad (2.12)$$

with $\alpha, \beta = 2, 3$ and $i = e, \mu, \tau$. As discussed earlier, N_1 being Z_2 odd remains stable, unlike the other two RHNs N_2 and N_3 , which can decay into the scalar and the SM leptons (l) through the third term of Eq. 2.12 if kinematically allowed. The existence of N_2 and N_3 in the present setup can also explain the origin of non-zero neutrino masses together with baryogenesis via leptogenesis. In addition, EWSB gives rise to the following mass matrix for $N_{1,2,3}$.

$$M_N = \sqrt{2} v_{BL} \begin{pmatrix} y_{11} & 0 & 0 \\ 0 & y_{22} & y_{23} \\ 0 & y_{23} & y_{33} \end{pmatrix}. \quad (2.13)$$

To demonstrate our point without losing the generality, we consider $y_{23} = 0$ for simplicity in the rest of the analysis, in which case M_N is diagonal with masses

$$M_i = \sqrt{2} y_{ii} v_{BL}. \quad (2.14)$$

For simplicity, we assume the other two RHNs to be nearly mass degenerate for the rest of the analysis and consider $y_{22} \simeq y_{33} = y$. Finally, for our analysis purpose, we choose the following sets of independent parameters:

$$\{m_s, M_1, y, v_{BL}, g_{BL}, s_\theta\}.$$

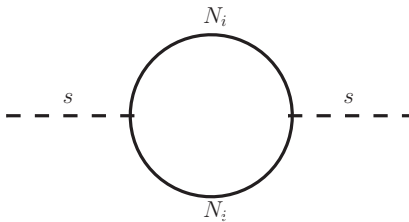


Figure 1: One-loop diagram contributing dominantly towards thermally corrected mass of scalar s .

3 Thermal corrections

This section briefly comments on the thermal corrections to the masses of relevant particles. These corrections play a non-trivial role in understanding the DM phenomenology of the present setup. In the early Universe, when the temperature of the thermal soup was very high, the thermal corrections [37, 74, 75] to the masses of the particles in the bath must have been very large. In general, any particle that couples in the thermal bath with the primordial plasma is expected to obtain a mass proportional to the temperature of the Universe provided the condition $T > m_i$ is satisfied, here m_i denotes various mass scales involved in the theory [76].

SM particles are expected to be in equilibrium with the thermal plasma at high temperatures. In the present set up we also assume that the particles like the scalar S and the heavier RHNs $N_{2,3}$ remained in equilibrium with the thermal plasma due to their sizable interaction strengths in the early Universe. Hence, their masses are expected to obtain thermal corrections at high temperature. On the other hand, DM candidate N_1 in this model interacts very feebly with the thermal bath and never enters thermal equilibrium. Due to this reason, the thermal correction to its mass remains negligible even at high temperatures. For example, considering $U(1)_{B-L}$ breaking scale $v_{BL} \sim \mathcal{O}(10^{10} \text{ GeV})$ with a fixed DM mass $M_1 \sim 500 \text{ GeV}$, one obtains $y_{11} \sim 3 \times 10^{-8} \text{ GeV}$, following Eq. 2.14. With such a feeble interaction, the thermal corrections to N_1 mass at a temperature $T \gg M_1$ remains negligible *i.e.* $M_1(T) = \sqrt{M_1^2 + (y_{11}^2/16)T^2} \simeq M_1$. Finally, the setup also demands a very feeble $g_{BL} \sim \mathcal{O}(10^{-8})$. Such a small g_{BL} also prevents Z_{BL} from entering into the equilibrium and hence its thermal mass can also be neglected. These choices of couplings will be further clarified in Section 5.

Now we discuss the thermal corrections to the mass of s as it plays a crucial role in the DM phenomenology of the present construct. Note that several processes can provide thermal contributions to the mass of s . For example, one can have self-energy corrections with s , H , Z_{BL} and N_i coming in the loop, which can contribute to the thermally corrected mass of s . These contributions can be denoted as $\Pi_s^2(T)$, $\Pi_H^2(T)$, $\Pi_{Z_{BL}}^2(T)$ and $\Pi_{N_i}^2(T)$ respectively. The present work demands a very large v_{BL} to ensure the feeble interaction of the DM with s . This, in turn, also makes the couplings like λ_S and $\lambda_{\phi S}$ negligibly small (see Eq. 2.11, with $v_{BL} \sim \mathcal{O}(10^{10} \text{ GeV})$, $\lambda_S \sim 10^{-13}$ and $\lambda_{\phi S} \sim 10^{-10}$). The smallness of these couplings guarantees that Π_s^2 , Π_H^2 remains significantly small in comparison to $\Pi_{N_i}^2(T)$ (Note that the $N_i - N_i - S$ coupling (y) can be quite large) and can be ignored. Next, the set up also demands a very small g_{BL} and hence the contributions of $\Pi_{Z_{BL}}^2(T)$ can also be safely ignored. The

thermal contribution to the mass of s from the diagram shown in Fig. 1 is given as [37, 74]:

$$\Pi_{N_i}^2(T) = \frac{y_i^2}{6} T^2. \quad (3.1)$$

Finally, the effective mass of the scalar can be expressed as,

$$M_s(T) = \sqrt{m_s^2 + \Pi_s^2(T) + \Pi_H^2(T) + \Pi_{Z_{BL}}^2(T) + \Pi_{N_i}^2(T)}. \quad (3.2)$$

One can similarly calculate the masses of $N_{2,3}$ in terms of temperature by incorporating all relevant contributions. In Section 5, we describe the importance of the thermal corrections in the context of the DM phenomenology.

4 Theoretical and experimental constraints

4.1 Theoretical constraints

The scalar potential discussed in Eq. 2.3 must remain bounded from below in various directions in the field space. Stability of vacuum can be ensured if the quartic couplings satisfy the following conditions:

$$\lambda_\phi > 0, \lambda_S > 0, \lambda_{\phi S} + \sqrt{2\lambda_\phi\lambda_S} > 0. \quad (4.1)$$

On the other hand, to keep the model parameters perturbative, the parameters must obey:

$$|\lambda_i| < 4\pi, |g_i| < \sqrt{4\pi}, |y_i| < \sqrt{4\pi}, \quad (4.2)$$

Where g_i and y_i denote the gauge, and the Yukawa couplings and λ_i represent the scalar quartic couplings involved in the calculation.

4.2 Experimental Constraints

- I. **Relic density and direct detection:** Due to the presence of a DM, the model is subjected to the constraints coming from the Planck experiment [3]:

$$\Omega_{\text{DM}} h^2 = 0.120 \pm 0.001. \quad (4.3)$$

Additionally, the model is also exposed to the constraints imposed by the direct detection experiments like LUX [16], PandaX-II [17] and Xenon-1T [18]. Elaborated discussions on the dark matter phenomenology are presented in Section 5.

- II. **LHC diphoton searches:** In presence of the mixing between h and s , the tree level interactions of the SM Higgs with the SM fermion and gauge bosons get modified. In such a scenario, the signal strength in the di-photon channel then takes a form:

$$\mu_{\gamma\gamma} = c_\theta^2 \frac{BR_{h \rightarrow \gamma\gamma}}{BR_{h \rightarrow \gamma\gamma}^{\text{SM}}} \simeq c_\theta^2 \frac{\Gamma_{h \rightarrow \gamma\gamma}}{\Gamma_{h \rightarrow \gamma\gamma}^{\text{SM}}}. \quad (4.4)$$

LHC sets a limit on this new mixing angle as $|\sin\theta| \leq 0.36$ [77].

III. **LEP bound and opposite sign di-lepton search at LHC:** Since the SM fermions are charged under $U(1)_{B-L}$ symmetry and interact directly with the $U(1)_{B-L}$ gauge boson Z_{BL} , the footprints of Z_{BL} can be obtained in the collider searches. The null detection of such signature severely constrains the ratio $M_{Z_{BL}}/g_{BL}$. The exclusion limit from LEP-II [78, 79] on this ratio is:

$$\frac{M_{Z_{BL}}}{g_{BL}} \geq 7 \text{ TeV}. \quad (4.5)$$

On the other hand, one should also observe the constraints coming from opposite-sign di-lepton searches at LHC, which primarily excludes the model for $150 \text{ GeV} < M_{Z_{BL}} < 3 \text{ TeV}$ [65, 80], depending on the size of g_{BL} . In this work, the $B-L$ gauge boson is treated as a FIMP which in turn demands g_{BL} to be very small, and hence the stringent constraints, as discussed above, can easily be evaded.

IV. **Invisible Higgs decay:** In this model, SM Higgs can also decay to the RHNs, Z_{BL} and also to the BSM scalar, if kinematically allowed. These extra decay modes can contribute towards invisible Higgs decay. In such a situation, we need to employ the bound on the invisible Higgs decay width as [81]:

$$Br(h \rightarrow \text{Invisible}) < 0.11, \quad (4.6a)$$

$$\frac{\Gamma(h \rightarrow \text{Invisible})}{\Gamma(h \rightarrow SM) + \Gamma(h \rightarrow \text{Invisible})} < 0.11. \quad (4.6b)$$

where $\Gamma(h \rightarrow \text{Invisible}) = \Gamma(h \rightarrow \text{BSM})$ when $m_i < \frac{m_h}{2}$ with $i = N_1, N_2, N_3, Z_{BL}, s$ and $\Gamma(h \rightarrow SM) = 4.2 \text{ MeV}$. However, in our present analysis, we primarily focus on the parameter space where $m_i > \frac{m_h}{2}$. So the above constraint is not applicable.

5 Dark Matter Phenomenology

Null detection of WIMP dark matter in the direct [16–18] and indirect search experiments [19] has motivated the community to explore the various exotic realization of DM. Among such possibilities, the popular one is the FIMP-type DM, where the DM never comes in equilibrium with the thermal soup. Here, the initial abundance of the DM is assumed to be zero (or negligible). As the Universe cools down, its feeble interaction with the bath helps in its gradual production from decays or scatterings of the bath particles. Such a weaker strength of coupling ensures that the DM interaction rate invariably remains smaller than the Hubble expansion rate (H), *i.e.* $\Gamma_{int} < H$. Studies of such a FIMP type DM establish a condition where the maximum DM production takes place when the temperature of the thermal bath is of the order or below the mass of the mother particle responsible for the production of the DM. Unlike the standard freeze-in scenario, in the present up, DM production can be enhanced at early times if thermal corrections to the mass of the mother particle are included. This mechanism of DM production can be dubbed as the *forbidden freeze-in*. Here, the DM production channel, which was otherwise forbidden or kinematically disallowed in the standard freeze-in (SFI), now becomes allowed once the thermal correction to the mass of the mother particle is incorporated.

The present setup explores the $U(1)_{B-L}$ extension of the SM where the lightest RHN (N_1), which is odd under a Z_2 symmetry, plays the role of FIMP dark matter. Here, the production of N_1 can take place from the decay of s, h (physical scalars obtained after

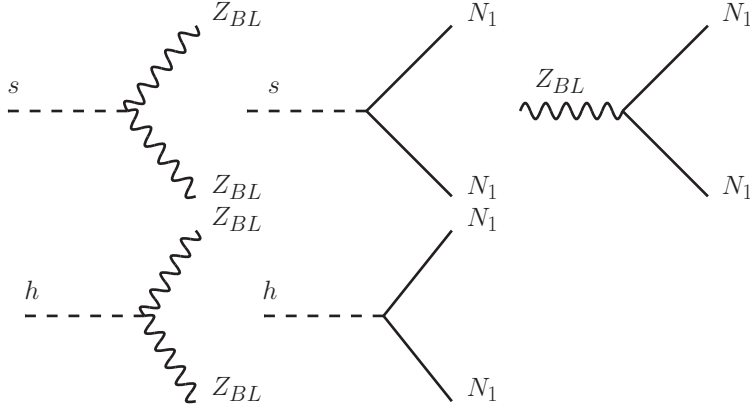


Figure 2: Possible production channels of Z_{BL} and the DM candidate N_1 .

the mixing between ϕ_S and ϕ_h after the EWSB) and Z_{BL} . All such relevant production channels of Z_{BL} and N_1 are depicted in Fig. 2. The feeble interaction of N_1 is assured by choosing a relatively large v_{BL} ($\Gamma_{s \rightarrow N_1 N_1} \propto y_{11}^2 c_\theta^2 \propto M_1^2 c_\theta^2 / v_{BL}^2$) and a relatively smaller g_{BL} ($\Gamma_{Z_{BL} \rightarrow N_1 N_1} \propto g_{BL}^2$). Note that, due to the smallness of g_{BL} , the $B - L$ gauge boson Z_{BL} also never thermalizes with bath and is produced feebly from the decay of s and h . Hence, in order to study the evolution of dark matter with the expansion of the Universe, one needs to solve a set of coupled Boltzmann equations while taking into account the evolution of Z_{BL} as well. The coupled Boltzmann equations are expressed as,

$$\frac{dY_{Z_{BL}}}{dx} = \frac{1}{Hx} \left[\theta(M_s(m_s/x) - 2M_{Z_{BL}}) \langle \Gamma_{s \rightarrow Z_{BL} Z_{BL}} \rangle Y_s^{EQ} - \langle \Gamma_{Z_{BL} \rightarrow all} \rangle Y_{Z_{BL}} \right], \quad (5.1a)$$

$$\frac{dY_{N_1}}{dx} = \frac{1}{Hx} \left[\langle \Gamma_{Z_{BL} \rightarrow N_1 N_1} \rangle Y_{Z_{BL}} + \theta(M_s(m_s/x) - 2M_1) \langle \Gamma_{s \rightarrow N_1 N_1} \rangle Y_s^{EQ} \right], \quad (5.1b)$$

Here $x = m_s/T$, where T and $H = 1.67 \sqrt{g_*} \frac{T^2}{M_{Pl}}$ denotes the temperature and expansion rate of the Universe respectively. Whereas $Y_j = n_j/\mathfrak{s}$ denotes the comoving number density of the different species ($j = s, Z_{BL}, N_1$) involved with \mathfrak{s} being the entropy density. Y_s^{EQ} signifies the equilibrium density of s . Next, $\langle \Gamma_i \rangle$ with $i = s, Z_{BL}$ represents the thermally averaged⁵ decay widths [28] where

$$\Gamma_{s \rightarrow Z_{BL} Z_{BL}} = \frac{g_{BL}^2 c_\theta^2}{8\pi} \frac{M_s^3(T)}{M_{Z_{BL}}^2} \left(1 - \frac{4M_{Z_{BL}}^2}{M_s^2(T)}\right)^{1/2} \left(1 - \frac{4M_{Z_{BL}}^2}{M_s^2(T)} + \frac{12M_{Z_{BL}}^4}{M_s^4(T)}\right), \quad (5.2a)$$

$$\Gamma_{s \rightarrow N_1 N_1} = \frac{M_s(T)}{32\pi} y_{11}^2 c_\theta^2 \left(1 - \frac{4M_1^2}{M_s^2(T)}\right)^{3/2}, \quad (5.2b)$$

$$\Gamma_{Z_{BL} \rightarrow N_1 N_1} = \frac{M_{Z_{BL}}}{24\pi} g_{BL}^2 \left(1 - \frac{4M_1^2}{M_{Z_{BL}}^2}\right)^{3/2}, \quad (5.2c)$$

⁵Since Z_{BL} never thermalizes with the plasma, one should properly consider the non-thermal distribution function ($f_{Z_{BL}}$) for Z_{BL} in order to calculate its thermally averaged decay width [28]. In such a scenario

$$\langle \Gamma_{Z_{BL}} \rangle = \frac{\int \left(\frac{M_{Z_{BL}}}{E_{Z_{BL}}}\right) \Gamma_{Z_{BL} \rightarrow AA} f_{Z_{BL}}(p, T) d^3p}{\int f_{Z_{BL}}(p, T) d^3p}.$$

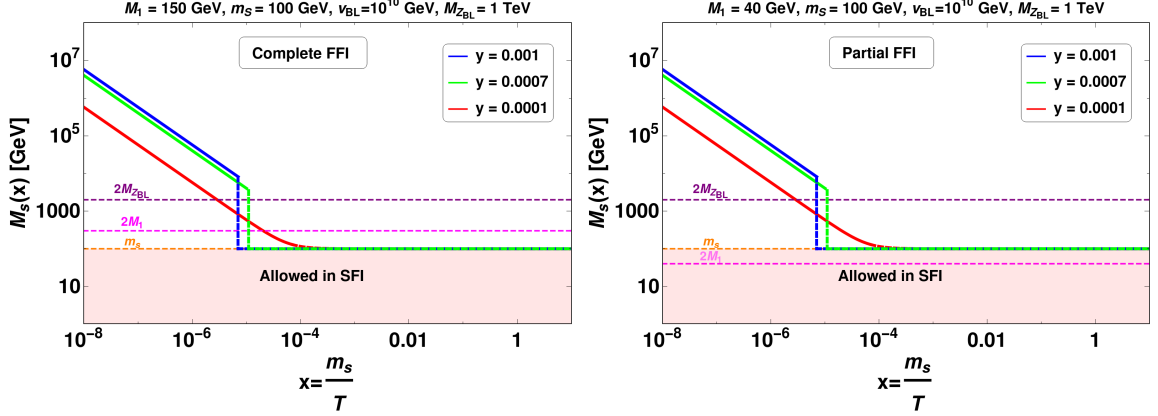


Figure 3: Variation of thermally corrected mass $M_s(x)$ of second scalar with a dimensionless quantity $x = \frac{m_s}{T}$ for three different values Yukawa coupling y . In the left panel, we demonstrate a scenario where the $B - L$ gauge boson Z_{BL} and the DM candidate N_1 can only be produced via the FFI mechanism. In contrast, the right panel depicts a picture where the Z_{BL} can only be produced via the FFI mechanism, but N_1 can be produced through both FFI and SFI.

$$\Gamma_{Z_{BL} \rightarrow f\bar{f}} = \frac{M_{Z_{BL}}}{12\pi} g_{BL}^2 \left(1 + \frac{2M_f^2}{M_{Z_{BL}}^2}\right) \left(1 - \frac{4M_f^2}{M_{Z_{BL}}^2}\right)^{1/2}. \quad (5.2d)$$

Note that, due to the large $B - L$ breaking scale, BSM particles gain their masses in the early Universe, and hence the Z_{BL} is mainly produced through the decay of s . At this stage, we would also like to mention that due to the feeble interaction (y_{11}) of the DM with s and large value of both s and N_i masses at high temperature the production of N_1 is dominated by the decay of s , while its production from scattering processes like $N_i N_i \rightarrow N_1 N_1$ or $hh(ss) \rightarrow N_1 N_1$ remains subdominant and can be neglected. Finally, we have also ensured that rate of the scattering processes like $N_1 N_i \rightarrow N_1 N_i$ and $N_1 h(s) \rightarrow N_1 h(s)$ remains several orders of magnitude smaller than the Hubble expansion rate. For example we found that $\Gamma_{N_1 N_i \rightarrow N_1 N_i} / H(T) \sim 10^{-20}$ at $T \simeq 10^8$ GeV which shows that the N_1 never enters thermal equilibrium even at high temperatures.

In the present setup, we are interested in exploring the production of both Z_{BL} and N_1 through the forbidden channels. These channels become effective once thermal corrections to the mass of s are incorporated and remain active only till the point these decays are kinematically allowed, this is ensured by the use of θ -function in Eq. 5.1. Once the asymptotic yield of the DM $Y_{N_1}(x_\infty)$ is obtained after solving the Boltzmann equation, we can use it to calculate the relic density of the DM as,

$$\Omega_{N_1} h^2 = 2.75 \times 10^8 \left(\frac{M_1}{\text{GeV}}\right) Y_{N_1}(x_\infty), \quad (5.3)$$

where x_∞ indicates the asymptotic value of x after the DM freeze-in.

To understand the DM phenomenology more evidently, we categorize our study into two cases in terms of possible mass hierarchies: (A) $M_{Z_{BL}} > M_1 > m_s$, and (B) $M_{Z_{BL}} > m_s > M_1$ so that the effect of FFI and its benefits over SFI becomes visible. We demonstrate the importance of these two cases in Fig. 3. Here, we show the variation of thermally corrected scalar mass $M_s(x)$ in terms of dimensionless parameter $x = m_s/T$ for three different choices

Decay-Channels	SFI	FFI
$s \rightarrow Z_{BL}Z_{BL}$	✗	✓
$s \rightarrow N_1N_1$	✗	✓
$Z_{BL} \rightarrow N_1N_1$	✗	✓

Table 2: List of processes contributing to dark matter and Z_{BL} production in a standard freeze-in (SFI) and forbidden freeze-in (FFI) scenario for a mass hierarchy $M_{Z_{BL}} > M_1 > m_s$. $s \rightarrow Z_{BL}Z_{BL}$ remains forbidden within this mass hierarchy for the SFI scenario, which in turn suggests that $Z_{BL} \rightarrow N_1N_1$ is also forbidden even though this decay remains kinematically allowed.

of Yukawa couplings y . Note that, while generating Fig. 3 we followed a conservative limit where it is assumed that the thermal correction to the mass of s remains significant till the temperature $T \sim M_{2,3} \sim yv_{BL}$. Below this temperature, the thermally corrected mass of s coincides with the bare mass value [76]. We follow the same principle in presenting the rest of our analysis. In Fig. 3 the dashed horizontal line represents the fixed values of different mass parameters, $2M_{Z_{BL}}$ (in purple), $2M_1$ (in magenta), and m_s (in orange) which helps to understand the mass hierarchy. The pink shaded region shows the parameter space where the FIMP type particles can also be produced if allowed in the SFI scenario. It is evident from the left panel of Fig. 3 that the production of the FIMP type particles (Z_{BL} and N_1) can only take place through the mechanism of FFI if one considers the mass hierarchy $M_{Z_{BL}} > M_1 > m_s$. On contrary to this, in the right panel of Fig. 3, we consider a situation where the mass of the dark matter *i.e.* M_1 lies below $M_s(T) = m_s$. Primary condition on scalar mass $M_s(T) = 2M_1$ ensures the production of the dark matter both from the decay of s and Z_{BL} in the forbidden freeze-in scenario and only through s in a standard freeze-in scenario. $s \rightarrow Z_{BL}Z_{BL}$ remains forbidden in this case due to the choice of mass hierarchy considered. This case also provides a clear distinction between the FFI and SFI scenarios. Next, we solve the set of coupled Boltzmann equations (Eq. 5.1) numerically to study the evolution of Z_{BL} and N_1 with the expansion of the Universe for these two cases.

5.1 Case A: Complete FFI region when $M_{Z_{BL}} > M_1 > m_s$

In this mass hierarchy, s being the lightest BSM particle, it neither decays to Z_{BL} nor to N_1 in a typical SFI scenario. Once the thermally corrected mass of s is taken into account, the left panel of Fig. 3 demonstrates that s can be heavy enough to produce both Z_{BL} and N_1 through the FFI mechanism. We also provide Table 2 for a better understanding of this picture.

To facilitate our discussion, in Fig. 4a, we show the variation of $Y_{Z_{BL}}$ and Y_{N_1} with a dimensionless quantity $x = \frac{m_s}{T}$. The values of different parameters controlling the DM phenomenology are mentioned at the top of each plot. One notices that the production of the Z_{BL} which can occur through the decay of the second scalar s is kinematically forbidden with the given choices of m_s and $M_{Z_{BL}}$ if the thermal corrections are not incorporated. Looking at the Eq. 2.11, one finds that for a large v_{BL} as required in this setup, the couplings λ_ϕ and $\lambda_{\phi S}$ remains significantly small, on the other hand, the setup also demands a very small g_{BL} ; hence the contribution of $\Pi_s^2(T)$, $\Pi_H^2(T)$ and $\Pi_{Z_{BL}}^2(T)$ in Eq. 3.2 remains almost negligible. On the other hand, the scalar field can acquire a sizeable thermal mass depending on the choices of BSM Yukawa couplings ($y_{22} \propto M_2/v_{BL}$ and $y_{33} \propto M_3/v_{BL}$). This is also consistent

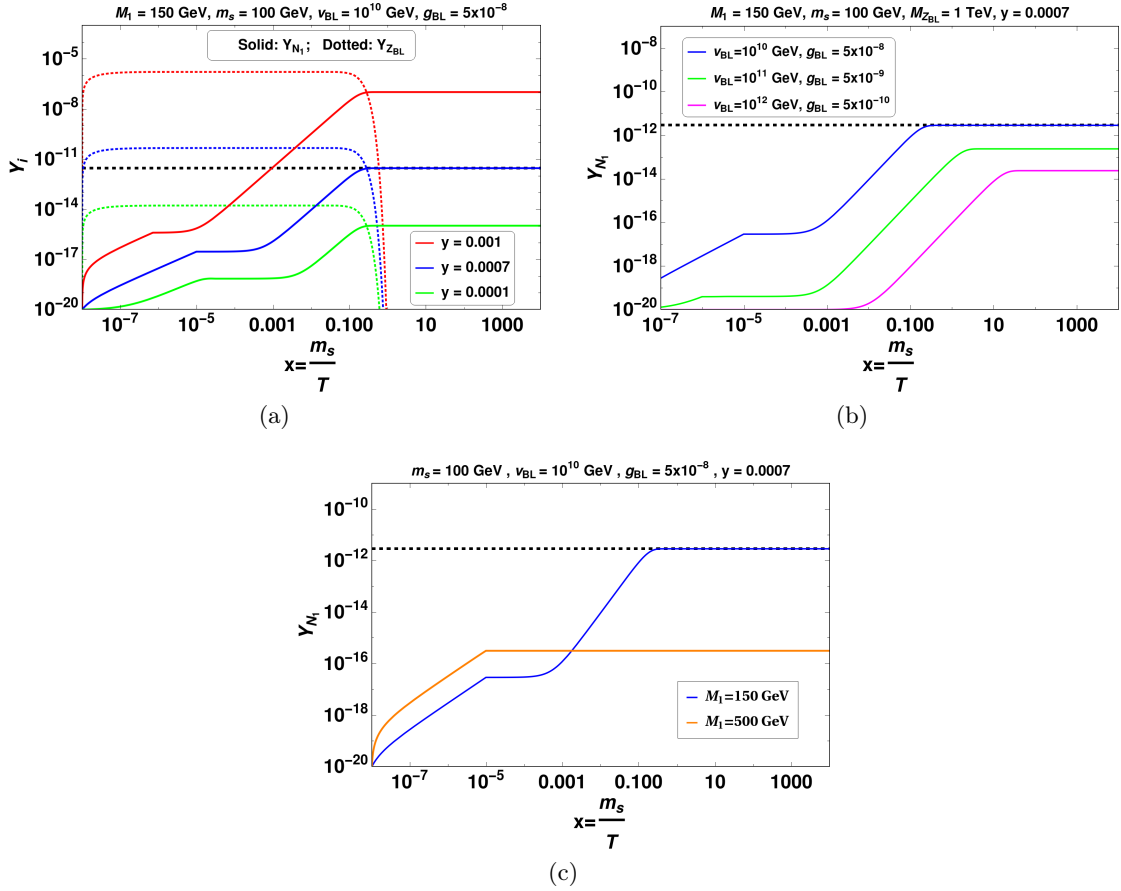


Figure 4: Evolution of generated yield of Z_{BL} (dotted lines) and dark matter N_1 (solid lines) with respect to a dimensionless parameter $x = \frac{m_s}{T}$. The values of different parameters controlling the DM phenomenology are mentioned at the top of each plot in a case study for complete FFI region, observed for mass hierarchy $M_{Z_{BL}} > M_1 > m_s$. Thick black dashed line represents the yield of the DM corresponding to the observed relic density.

with our expectation that the masses of the other two RHNs must be quite heavy to explain the non-zero neutrino masses and leptogenesis through Type-I seesaw. It is expected that, with an adequate choice of the y (with $y_{22} \simeq y_{33} = y$), one can easily obtain a scenario: $M_s(T) > 2M_{Z_{BL}}, 2M_1$ and thereafter, the decay of s can produce Z_{BL} and N_1 . This can also be seen in Fig. 4a. Next, with the choices of parameters considered, the production of N_1 can also proceed via the decay of Z_{BL} . In Fig. 4a, the evolution of Z_{BL} (dotted) and N_1 (solid) are shown for three different choices of y , *i.e.* $y = 10^{-3}$ (red), $y = 7 \times 10^{-4}$ (blue), $y = 10^{-4}$ (green). With $y = 10^{-3}$, the thermally corrected mass of s is expected to be large. The larger mass leads to a relatively larger decay widths for the processes $s \rightarrow Z_{BL}Z_{BL}$ and $s \rightarrow N_1N_1$ (in comparison to smaller y values) which in turn generates relatively larger yields of Z_{BL} and N_1 in Fig. 4a. One notices that the abundance of Z_{BL} gradually increases due to its production from the decay of s , then saturates (plateau) once its production rate becomes comparable to its decay rate. Finally, it falls as its decay to the SM fermions, and the DM overtakes its production. However, the abundance of N_1 increases slowly till the time (first bend) when

Decay-Channels	SFI	FFI
$s \rightarrow Z_{BL}Z_{BL}$	✗	✓
$s \rightarrow N_1N_1$	✓	✓
$Z_{BL} \rightarrow N_1N_1$	✗	✓

Table 3: List of processes contributing to dark matter production in a standard freeze-in (SFI) and forbidden freeze-in (FFI) scenario for a mass hierarchy $M_{Z_{BL}} > m_s > M_1$. $s \rightarrow Z_{BL}Z_{BL}$ remains forbidden within this mass hierarchy for the SFI scenario, which in turn suggests that $Z_{BL} \rightarrow N_1N_1$ is also forbidden even though this decay remains kinematically allowed.

the temperature of the Universe becomes of the order of the heavier RHN masses *i.e.* $T \simeq M_i$ (*i.e.* $x \simeq 7 \times 10^{-6}$ for $y = 0.001$), after which its production from the decay of s becomes kinematically forbidden, and its yield saturates. This is because, at this point, the dominant contribution to the thermally corrected mass of s becomes insignificant (as also discussed in Section 3), and $M_s(T)$ falls back to the bare mass value m_s . Subsequently, a relatively sharper rise is observed in its yield due to its production from Z_{BL} , and finally, its abundance saturates (at around $T \simeq M_{Z_{BL}}$ *i.e.* $x \simeq 10^{-1}$) once the decay of Z_{BL} is completed. It is interesting to point out that the production of Z_{BL} from the decay of s starts much earlier in comparison to the production of N_1 . This happens because the s decays dominantly to Z_{BL} and sub-dominantly to N_1 (see Eq. 5.2). Similar behavior is observed in the evolution of Z_{BL} for smaller y , but with a relatively smaller yield. With a small y , the thermal correction to the mass of s also remains small. This, in turn, reduces the decay width of s . Unlike the scenario with a relatively larger y , now N_1 production ceases when the decay $s \rightarrow N_1N_1$ becomes kinematically disallowed at a relatively later time (as a smaller y corresponds to a smaller value of $M_{2,3}$, hence a larger x). It again starts getting produced as the $Z_{BL} \rightarrow N_1N_1$ becomes operational. Finally, DM abundance freezes in once the decay of Z_{BL} is complete. The thick dashed horizontal black line (in each plot) indicates the abundance of dark matter for which the relic density satisfies the Planck experimental limit.

Next, in Fig. 4b we show the evolution of the dark matter for three different combinations of v_{BL} and g_{BL} while keeping $M_{Z_{BL}}$ fixed at 1 TeV. Here, one finds that for a choice of smaller v_{BL} (and a larger g_{BL}), both the FFI production channels get enhanced, leading to an overabundant N_1 (as $\Gamma(s \rightarrow N_1N_1) \propto \frac{1}{v_{BL}^2}$ and $\Gamma(Z_{BL} \rightarrow N_1N_1) \propto g_{BL}^2$). Hence, one can accommodate the correct yield of the DM by tuning these two parameters appropriately, as seen from the blue curve. Lastly, Fig. 4c shows the effect of different DM masses on its evolution. For a choice with $M_1 = 500$ GeV, the only source of its production is the decay of s . The moment this decay stops, the DM yield becomes constant. In such a case, it is difficult for the DM to satisfy the measured relic at the Planck experiment.

5.2 Case B: Partial FFI region when $M_{Z_{BL}} > m_s > M_1$

We now aim to study the DM phenomenology with the above mass hierarchy where FFI decay modes are open partially, as also shown in the right panel of Fig 3. Hence evolution process of the DM indicates a distinct direction in the FFI scenario compared to SFI. Unlike the previous case, DM can now be produced directly from the decay of s , even if $M_s(T) \simeq m_s$ is satisfied. However, the production of the Z_{BL} can only be possible through the forbidden

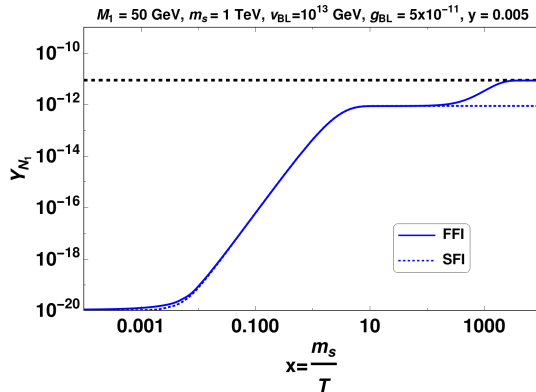


Figure 5: Evolution of generated yield of N_1 with respect to a dimensionless parameter $x = \frac{m_s}{T}$. The solid blue line depicts the production of N_1 in an FFI scenario which can satisfy the Planck experimental limit on the relic density for the given choice of parameters. With the same choice of parameters, the DM remains under-abundant for an SFI scenario, as shown by the dashed blue line. The values of different parameters controlling the DM phenomenology are mentioned at the top of each plot in a case study for partial FFI region, observed for mass hierarchy $M_{Z_{BL}} > m_s > M_1$. The thick black dashed line represents the abundance of the DM corresponding to the observed relic density.

freeze-in mechanism from the decay of s ⁶. For a better understanding, in Table 3 we provide all the relevant decay channels required for the production of Z_{BL} and N_1 for FFI and SFI. Next, we demonstrate the importance of forbidden freeze-in (FFI) over the standard freeze-in (SSI) in Fig. 5.

This figure shows a comparison between the production of the DM in the SFI scenario (dashed blue line) and the FFI scenario (solid blue line). Here, with the given choice of parameters, the Z_{BL} can never be produced from the decay of s in the SFI scenario. Hence its abundance remains almost negligible (as it can also be produced through scatterings). With such an insignificant yield, Z_{BL} contribution in producing the DM will always remain sub-dominant in comparison to the DM production coming from the s decay. Hence, the DM yield saturates as soon as its production from the s decay stops. In this situation, it may become difficult for the DM to satisfy the correct order of relic density. On the other hand, with the incorporation of FFI, DM can be further produced from the decay of both s and Z_{BL} in an adequate amount to satisfy the correct relic density with the given choice of parameters.

Finally, we also like to comment on the detection prospect of the model under consideration. The spontaneous breaking of the $U(1)_{B-L}$ symmetry at a high energy scale leads to the formation of Nambu-Goto *cosmic strings* [82]. Once formed, the collisions and self-interactions of strings produce non-self-interacting string loops, which further oscillates and radiates their energy in the form of gravitational wave (GW). The incoherent superposition of such continuous emission results in stochastic GW signals. This GW signal can be detected at the present and future GW detectors like pulsar timing arrays (PTAs), NANOGrav [83], PPTA [84], EPTA [85], IPTA [86], LISA [87], LIGO [88] etc. The searches of GWs can increase the predictability of the present setup. The detailed study of GWs is beyond the scope

⁶Although the production of Z_{BL} can proceed through $2 \rightarrow 2$ scatterings, its abundance remains almost negligible as the production cross-section depends on g_{BL}^4 .

of the present work, and we plan to take it as a future endeavor.

6 Summary and conclusions

In this paper, we study the phenomenology of feebly interacting massive particles as dark matter in a minimal $U(1)_{B-L}$ extension of the SM. The role of DM is played by the lightest of the three right-handed neutrinos, which in turn are introduced to make the model free from the triangular anomaly. The other two heavier RHNs can generate non-zero neutrino masses and matter-antimatter asymmetry of the Universe through Type-I seesaw. Here, an unbroken Z_2 symmetry ensures the stability of the DM. The setup also requires a complex $SU(2)_L$ singlet scalar charged under the $B-L$ symmetry. After obtaining a non-zero vev, the scalar breaks the $U(1)_{B-L}$ spontaneously and simultaneously makes the RHNs together with a $B-L$ gauge boson massive.

Due to their feeble interactions with the bath particles, both the DM candidate (N_1) and $B-L$ gauge boson (Z_{BL}) never comes in equilibrium with the thermal bath. Contrary to this, the complex scalar mediator remains in the thermal equilibrium with the bath due to its not-so-small interactions with the bath particles and contributes to the gradual freeze-in production of N_1 and Z_{BL} . Moreover, if kinematically allowed, the DM production is further dominated by the Z_{BL} decay.

Although FIMP-type DM is studied in the $B-L$ framework, the thermal corrections to the mediator masses were never taken into account. Incorporating such corrections to the mediator mass at high temperature opens up a new paradigm for a FIMP-type DM phenomenology. Simultaneously, it also opens up an attractive possibility of producing the DM in a kinematically forbidden region of the standard freeze-in (SFI) picture. In this work, we explore this exciting possibility. With this in mind, we categorized our study into two cases depending on the mass hierarchy of these particles. All other likely mass hierarchies can be summed up within these two possibilities.

The first illustration depicts a forbidden freeze-in (FFI) picture where gauge boson and dark matter are heavier than the complex scalar residing in the thermal bath. Hence, the decay is kinematically disallowed, and consequently, such a picture is utterly missing in the SFI framework. The appealing feature here is that the production of the DM can take place in two steps: first from the decay of the scalar due to the thermal corrections to its mass and then subsequently from the late time decay of the gauge boson. Our example explores the synergy between these two processes depending upon parameters in the model.

For further clarity, in our second case study, we choose a particular mass hierarchy ($M_{Z_{BL}} > m_s > M_1$) to mark the role of FFI over SFI scenarios. Here the production of Z_{BL} is kinematically forbidden in the SFI case, while the dark matter is produced only from $B-L$ scalar's decay. Unlike the standard scenario, with the help of a large thermally corrected mass in FFI, the scalar can produce the gauge boson together with the dark matter in the early Universe. Similar to the first scenario, the DM production again happens in two steps which makes the distinction of FFI with SFI noticeable. Finally, due to the involvement of a large $B-L$ breaking scale, the model can be tested indirectly in the GW search experiments. Such a scale leads to the formation of cosmic string, which further oscillates and radiates its energy in the form of gravitational waves.

Acknowledgments

This work is supported by the Physical Research Laboratory (PRL), Department of Space, Government of India. Computational work was performed using the HPC resources (Vikram-100 HPC) and TDP project at PRL. Authors gratefully thank H. Mishra for stimulating discussions during the project.

References

- [1] Y. Sofue and V. Rubin, *Rotation curves of spiral galaxies*, *Ann. Rev. Astron. Astrophys.* **39** (2001) 137 [[astro-ph/0010594](#)].
- [2] D. Clowe, M. Bradac, A. H. Gonzalez, M. Markevitch, S. W. Randall, C. Jones et al., *A direct empirical proof of the existence of dark matter*, *Astrophys. J. Lett.* **648** (2006) L109 [[astro-ph/0608407](#)].
- [3] PLANCK collaboration, *Planck 2018 results. VI. Cosmological parameters*, *Astron. Astrophys.* **641** (2020) A6 [[1807.06209](#)].
- [4] G. Hinshaw, D. Larson, E. Komatsu, D. N. Spergel, C. L. Bennett, J. Dunkley et al., *Nine-year wilkinson microwave anisotropy probe (wmap) observations: Cosmological parameter results*, *The Astrophysical Journal Supplement Series* **208** (2013) 19.
- [5] D. Borah, R. Roshan and A. Sil, *Minimal two-component scalar doublet dark matter with radiative neutrino mass*, *Phys. Rev. D* **100** (2019) 055027 [[1904.04837](#)].
- [6] S. Bhattacharya, N. Chakrabarty, R. Roshan and A. Sil, *Multicomponent dark matter in extended $U(1)_{B-L}$: neutrino mass and high scale validity*, *JCAP* **04** (2020) 013 [[1910.00612](#)].
- [7] P. Konar, A. Mukherjee, A. K. Saha and S. Show, *Linking pseudo-Dirac dark matter to radiative neutrino masses in a singlet-doublet scenario*, *Phys. Rev. D* **102** (2020) 015024 [[2001.11325](#)].
- [8] D. Borah, R. Roshan and A. Sil, *Sub-TeV singlet scalar dark matter and electroweak vacuum stability with vectorlike fermions*, *Phys. Rev. D* **102** (2020) 075034 [[2007.14904](#)].
- [9] P. Konar, A. Mukherjee, A. K. Saha and S. Show, *A dark clue to seesaw and leptogenesis in a pseudo-Dirac singlet doublet scenario with (non)standard cosmology*, *JHEP* **03** (2021) 044 [[2007.15608](#)].
- [10] A. Dutta Banik, R. Roshan and A. Sil, *Two component singlet-triplet scalar dark matter and electroweak vacuum stability*, *Phys. Rev. D* **103** (2021) 075001 [[2009.01262](#)].
- [11] N. Chakrabarty, R. Roshan and A. Sil, *Two Component Doublet-Triplet Scalar Dark Matter stabilising the Electroweak vacuum*, [2102.06032](#).
- [12] B. Barman, N. Bernal, A. Das and R. Roshan, *Non-minimally Coupled Vector Boson Dark Matter*, [2108.13447](#).
- [13] A. Bhardwaj, A. Das, P. Konar and A. Thalappillil, *Looking for Minimal Inverse Seesaw scenarios at the LHC with Jet Substructure Techniques*, *J. Phys. G* **47** (2020) 075002 [[1801.00797](#)].
- [14] A. Bhardwaj, P. Konar, T. Mandal and S. Sadhukhan, *Probing the inert doublet model using jet substructure with a multivariate analysis*, *Phys. Rev. D* **100** (2019) 055040 [[1905.04195](#)].
- [15] L. Heurtier and H. Partouche, *Spontaneous Freeze Out of Dark Matter From an Early Thermal Phase Transition*, *Phys. Rev. D* **101** (2020) 043527 [[1912.02828](#)].
- [16] LUX collaboration, *Results from a search for dark matter in the complete LUX exposure*, *Phys. Rev. Lett.* **118** (2017) 021303 [[1608.07648](#)].

- [17] PANDAX collaboration, *Dark matter direct search sensitivity of the PandaX-4T experiment*, *Sci. China Phys. Mech. Astron.* **62** (2019) 31011 [[1806.02229](#)].
- [18] XENON collaboration, *Dark Matter Search Results from a One Ton-Year Exposure of XENON1T*, *Phys. Rev. Lett.* **121** (2018) 111302 [[1805.12562](#)].
- [19] MAGIC, FERMI-LAT collaboration, *Limits to Dark Matter Annihilation Cross-Section from a Combined Analysis of MAGIC and Fermi-LAT Observations of Dwarf Satellite Galaxies*, *JCAP* **02** (2016) 039 [[1601.06590](#)].
- [20] CMS collaboration, *Observation of a New Boson at a Mass of 125 GeV with the CMS Experiment at the LHC*, *Phys. Lett.* **B716** (2012) 30 [[1207.7235](#)].
- [21] ATLAS collaboration, *Observation of a new particle in the search for the Standard Model Higgs boson with the ATLAS detector at the LHC*, *Phys. Lett.* **B716** (2012) 1 [[1207.7214](#)].
- [22] L. J. Hall, K. Jedamzik, J. March-Russell and S. M. West, *Freeze-In Production of FIMP Dark Matter*, *JHEP* **03** (2010) 080 [[0911.1120](#)].
- [23] N. Bernal, M. Heikinheimo, T. Tenkanen, K. Tuominen and V. Vaskonen, *The Dawn of FIMP Dark Matter: A Review of Models and Constraints*, *Int. J. Mod. Phys. A* **32** (2017) 1730023 [[1706.07442](#)].
- [24] F. Elahi, C. Kolda and J. Unwin, *UltraViolet Freeze-in*, *JHEP* **03** (2015) 048 [[1410.6157](#)].
- [25] A. Biswas, S. Ganguly and S. Roy, *Fermionic dark matter via UV and IR freeze-in and its possible X-ray signature*, *JCAP* **03** (2020) 043 [[1907.07973](#)].
- [26] B. Barman, D. Borah and R. Roshan, *Effective Theory of Freeze-in Dark Matter*, *JCAP* **11** (2020) 021 [[2007.08768](#)].
- [27] B. Barman, D. Borah and R. Roshan, *Nonthermal leptogenesis and UV freeze-in of dark matter: Impact of inflationary reheating*, *Phys. Rev. D* **104** (2021) 035022 [[2103.01675](#)].
- [28] A. Biswas and A. Gupta, *Freeze-in Production of Sterile Neutrino Dark Matter in $U(1)_{B-L}$ Model*, *JCAP* **09** (2016) 044 [[1607.01469](#)].
- [29] A. Datta, R. Roshan and A. Sil, *Imprint of the seesaw mechanism on feebly interacting dark matter and the baryon asymmetry*, [2104.02030](#).
- [30] G. Bélanger, S. Khan, R. Padhan, M. Mitra and S. Shil, *Right handed neutrinos, TeV scale BSM neutral Higgs boson, and FIMP dark matter in an EFT framework*, *Phys. Rev. D* **104** (2021) 055047 [[2104.04373](#)].
- [31] S. Bhattacharya, R. Roshan, A. Sil and D. Vatsyayan, *Symmetry origin of Baryon Asymmetry, Dark Matter and Neutrino Mass*, [2105.06189](#).
- [32] L. Darmé, A. Hryczuk, D. Karamitros and L. Roszkowski, *Forbidden frozen-in dark matter*, *JHEP* **11** (2019) 159 [[1908.05685](#)].
- [33] E. Braaten and D. Segel, *Neutrino energy loss from the plasma process at all temperatures and densities*, *Phys. Rev. D* **48** (1993) 1478 [[hep-ph/9302213](#)].
- [34] H. Eberl, I. D. Gialamas and V. C. Spanos, *Gravitino thermal production revisited*, *Phys. Rev. D* **103** (2021) 075025 [[2010.14621](#)].
- [35] V. S. Rychkov and A. Strumia, *Thermal production of gravitinos*, *Phys. Rev. D* **75** (2007) 075011 [[hep-ph/0701104](#)].
- [36] A. Strumia, *Thermal production of axino Dark Matter*, *JHEP* **06** (2010) 036 [[1003.5847](#)].
- [37] M. J. Baker, M. Breitbach, J. Kopp and L. Mittnacht, *Dynamic Freeze-In: Impact of Thermal Masses and Cosmological Phase Transitions on Dark Matter Production*, *JHEP* **03** (2018) 114 [[1712.03962](#)].

- [38] S. Biondini and J. Ghiglieri, *Freeze-in produced dark matter in the ultra-relativistic regime*, *JCAP* **03** (2021) 075 [2012.09083].
- [39] A. Davidson, *$b - l$ as the fourth color within an $SU(2)_L \times U(1)_R \times U(1)$ model*, *Phys. Rev. D* **20** (1979) 776.
- [40] R. Marshak and R. Mohapatra, *Quark-lepton symmetry and $b - l$ as the $u(1)$ generator of the electroweak symmetry group*, *Physics Letters B* **91** (1980) 222.
- [41] R. N. Mohapatra and R. E. Marshak, *Local $B-L$ Symmetry of Electroweak Interactions, Majorana Neutrinos and Neutron Oscillations*, *Phys. Rev. Lett.* **44** (1980) 1316.
- [42] A. Davidson and K. C. Wali, *Universal seesaw mechanism?*, *Phys. Rev. Lett.* **59** (1987) 393.
- [43] A. Biswas, S. Choubey and S. Khan, *Galactic gamma ray excess and dark matter phenomenology in a $U(1)_{B-L}$ model*, *JHEP* **08** (2016) 114 [1604.06566].
- [44] A. Biswas, S. Choubey and S. Khan, *Neutrino mass, leptogenesis and FIMP dark matter in a $U(1)_{B-L}$ model*, *Eur. Phys. J. C* **77** (2017) 875 [1704.00819].
- [45] P. Fileviez Pérez, C. Murgui and A. D. Plascencia, *Neutrino-Dark Matter Connections in Gauge Theories*, *Phys. Rev. D* **100** (2019) 035041 [1905.06344].
- [46] W. Abdallah, S. Choubey and S. Khan, *FIMP dark matter candidate(s) in a $B - L$ model with inverse seesaw mechanism*, *JHEP* **06** (2019) 095 [1904.10015].
- [47] P. Bandyopadhyay, M. Mitra and A. Roy, *Relativistic freeze-in with scalar dark matter in a gauged $B - L$ model and electroweak symmetry breaking*, *JHEP* **05** (2021) 150 [2012.07142].
- [48] P. Minkowski, *$\mu \rightarrow e\gamma$ at a Rate of One Out of 10^9 Muon Decays?*, *Phys. Lett. B* **67** (1977) 421.
- [49] M. Gell-Mann, P. Ramond and R. Slansky, *Complex Spinors and Unified Theories*, *Conf. Proc. C* **790927** (1979) 315 [1306.4669].
- [50] R. N. Mohapatra and G. Senjanovic, *Neutrino Mass and Spontaneous Parity Nonconservation*, *Phys. Rev. Lett.* **44** (1980) 912.
- [51] T. Yanagida, *Horizontal Symmetry and Masses of Neutrinos*, *Progress of Theoretical Physics* **64** (1980) 1103 [https://academic.oup.com/ptp/article-pdf/64/3/1103/5394376/64-3-1103.pdf].
- [52] J. Schechter and J. W. F. Valle, *Neutrino Masses in $SU(2) \times U(1)$ Theories*, *Phys. Rev. D* **22** (1980) 2227.
- [53] J. Schechter and J. W. F. Valle, *Neutrino Decay and Spontaneous Violation of Lepton Number*, *Phys. Rev. D* **25** (1982) 774.
- [54] V. Brdar, A. J. Helmboldt, S. Iwamoto and K. Schmitz, *Type-I Seesaw as the Common Origin of Neutrino Mass, Baryon Asymmetry, and the Electroweak Scale*, *Phys. Rev. D* **100** (2019) 075029 [1905.12634].
- [55] SUPER-KAMIOKANDE collaboration, *Evidence for oscillation of atmospheric neutrinos*, *Phys. Rev. Lett.* **81** (1998) 1562 [hep-ex/9807003].
- [56] SNO collaboration, *Direct evidence for neutrino flavor transformation from neutral current interactions in the Sudbury Neutrino Observatory*, *Phys. Rev. Lett.* **89** (2002) 011301 [nucl-ex/0204008].
- [57] G. L. Fogli, E. Lisi, A. Marrone, A. Palazzo and A. M. Rotunno, *Neutrino masses and neutrino mixing*, *Nucl. Phys. B Proc. Suppl.* **155** (2006) 5.
- [58] K2K collaboration, *Indications of neutrino oscillation in a 250 km long baseline experiment*, *Phys. Rev. Lett.* **90** (2003) 041801 [hep-ex/0212007].
- [59] M. Fukugita and T. Yanagida, *Baryogenesis Without Grand Unification*, *Phys. Lett. B* **174** (1986) 45.

- [60] M. Plumacher, *Baryogenesis and lepton number violation*, *Z. Phys. C* **74** (1997) 549 [[hep-ph/9604229](#)].
- [61] A. Riotto and M. Trodden, *Recent progress in baryogenesis*, *Ann. Rev. Nucl. Part. Sci.* **49** (1999) 35 [[hep-ph/9901362](#)].
- [62] M. Dine and A. Kusenko, *The Origin of the matter - antimatter asymmetry*, *Rev. Mod. Phys.* **76** (2003) 1 [[hep-ph/0303065](#)].
- [63] A. Dutta Banik, R. Roshan and A. Sil, *Neutrino mass and asymmetric dark matter: study with inert Higgs doublet and high scale validity*, *JCAP* **03** (2021) 037 [[2011.04371](#)].
- [64] A. Datta, R. Roshan and A. Sil, *Scalar Triplet Flavor Leptogenesis with Dark Matter*, [2110.03914](#).
- [65] M. Escudero, S. J. Witte and N. Rius, *The dispirited case of gauged $U(1)_{B-L}$ dark matter*, *JHEP* **08** (2018) 190 [[1806.02823](#)].
- [66] T. Basak and T. Mondal, *Constraining Minimal $U(1)_{B-L}$ model from Dark Matter Observations*, *Phys. Rev. D* **89** (2014) 063527 [[1308.0023](#)].
- [67] N. Okada and O. Seto, *Higgs portal dark matter in the minimal gauged $U(1)_{B-L}$ model*, *Phys. Rev. D* **82** (2010) 023507 [[1002.2525](#)].
- [68] S. Khalil and O. Seto, *Sterile neutrino dark matter in $B - L$ extension of the standard model and galactic 511-keV line*, *JCAP* **10** (2008) 024 [[0804.0336](#)].
- [69] O. Seto and T. Shimomura, *Signal from sterile neutrino dark matter in extra $U(1)$ model at direct detection experiment*, *Phys. Lett. B* **811** (2020) 135880 [[2007.14605](#)].
- [70] Q. Decant, J. Heisig, D. C. Hooper and L. Lopez-Honorez, *Lyman- α constraints on freeze-in and superWIMPs*, [2111.09321](#).
- [71] J. C. Montero and V. Pleitez, *Gauging $U(1)$ symmetries and the number of right-handed neutrinos*, *Phys. Lett. B* **675** (2009) 64 [[0706.0473](#)].
- [72] A. Hook, E. Izaguirre and J. G. Wacker, *Model Independent Bounds on Kinetic Mixing*, *Adv. High Energy Phys.* **2011** (2011) 859762 [[1006.0973](#)].
- [73] LHC HIGGS CROSS SECTION WORKING GROUP collaboration, *Handbook of LHC Higgs Cross Sections: 4. Deciphering the Nature of the Higgs Sector*, [1610.07922](#).
- [74] M. E. Carrington, *Effective potential at finite temperature in the standard model*, *Phys. Rev. D* **45** (1992) 2933.
- [75] G. F. Giudice, A. Notari, M. Raidal, A. Riotto and A. Strumia, *Towards a complete theory of thermal leptogenesis in the SM and MSSM*, *Nucl. Phys. B* **685** (2004) 89 [[hep-ph/0310123](#)].
- [76] D. Comelli and J. R. Espinosa, *Bosonic thermal masses in supersymmetry*, *Phys. Rev. D* **55** (1997) 6253 [[hep-ph/9606438](#)].
- [77] T. Robens and T. Stefaniak, *LHC Benchmark Scenarios for the Real Higgs Singlet Extension of the Standard Model*, *Eur. Phys. J. C* **76** (2016) 268 [[1601.07880](#)].
- [78] M. Carena, A. Daleo, B. A. Dobrescu and T. M. P. Tait, *Z' gauge bosons at the Tevatron*, *Phys. Rev. D* **70** (2004) 093009 [[hep-ph/0408098](#)].
- [79] G. Cacciapaglia, C. Csaki, G. Marandella and A. Strumia, *The Minimal Set of Electroweak Precision Parameters*, *Phys. Rev. D* **74** (2006) 033011 [[hep-ph/0604111](#)].
- [80] A. Das, P. S. B. Dev, Y. Hosotani and S. Mandal, *Probing the minimal $U(1)_X$ model at future electron-positron colliders via the fermion pair-production channel*, [2104.10902](#).
- [81] ATLAS collaboration, *Combination of searches for invisible Higgs boson decays with the ATLAS experiment*, .

- [82] L. Bian, X. Liu and K.-P. Xie, *Probing superheavy dark matter with gravitational waves*, [2107.13112](#).
- [83] M. A. McLaughlin, *The North American Nanohertz Observatory for Gravitational Waves*, *Class. Quant. Grav.* **30** (2013) 224008 [[1310.0758](#)].
- [84] R. M. Shannon et al., *Gravitational waves from binary supermassive black holes missing in pulsar observations*, *Science* **349** (2015) 1522 [[1509.07320](#)].
- [85] M. Kramer and D. J. Champion, *The European Pulsar Timing Array and the Large European Array for Pulsars*, *Class. Quant. Grav.* **30** (2013) 224009.
- [86] G. Hobbs et al., *The international pulsar timing array project: using pulsars as a gravitational wave detector*, *Class. Quant. Grav.* **27** (2010) 084013 [[0911.5206](#)].
- [87] LISA collaboration, *Laser Interferometer Space Antenna*, [1702.00786](#).
- [88] LIGO SCIENTIFIC, VIRGO collaboration, *Search for the isotropic stochastic background using data from Advanced LIGO's second observing run*, *Phys. Rev. D* **100** (2019) 061101 [[1903.02886](#)].